Notion on the Correct Use of the Robot Effective Mass in the Safety Context and Comments on ISO/TS 15066

Robin Jeanne Kirschner, Nico Mansfeld, Guillermo Gómez Peña, Saeed Abdolshah and Sami Haddadin

***Abstract*— Collision experiments in the human-robot interaction (HRI) context showed that the effective robot mass is one of the main parameters that influence human injury probability during a collision. Also the current standard ISO/TS 15066 highlights the importance of this parameter and provides a method to determine the maximum safe robot velocity based on the effective mass. To enable both safe and efficient robot applications, it is crucial to derive the robot's instantaneous effective mass sufficiently accurate based on either a), a kinematic and dynamic model or b), a suitable collision experiment. In this paper, we describe and quantitatively compare the well-established reflected mass model by Khatib and the simplified model provided in the ISO/TS 15066 for the KUKA LWR IV+ and the Franka Emika Panda robot. Furthermore, we propose a method to practically determine the effective mass using a passive mechanical pendulum setup. Our results show that the simplified ISO/TS model can lead to a significant safety-relevant error. With our preliminary experimental setup, however, we can verify that the reflected mass obtained by the dynamics model only differs $1.1 - 7.8\,\%$ from the measured value.**

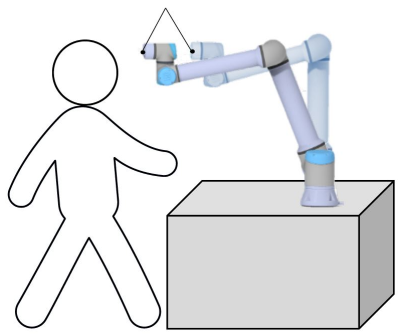

Fig. 1. The robot effective mass is a crucial parameter for safety assessment and safe control in HRI.

I. INTRODUCTION

A primary concern in human-robot interaction (HRI) is to ensure human safety even in dynamic, partially unknown environments. Many efforts have been taken to understand the collision dynamics in different contact scenarios [1], [2], [3]. The human injury probability during a collision is influenced by several robot parameters, e.g., the robot kinematic and inertial properties, the impact velocity, the surface properties (blunt/edgy, rigid/elastic, etc.), and the joint/link stiffness [4], [6]. In [10], [5], comprehensive collision experiments were conducted with crash-test dummies and soft tissue, where the role of the robot's reflected mass [8], i.e., the mass perceived during a collision, and velocity was investigated. In [10], the data-driven relation *(reflected mass, velocity, contact curvature)* $\rightarrow$ *injury* was established and systematic biomechanical impact experiments were carried out. So-called safety curves were derived from the experimental results, which relate the instantaneous robot reflected mass and contact geometry to a biomechanically safe velocity, which can be commanded to the robot. Such safety curves are also included in the current standard ISO/TS 15066:2016 (ISO/TS). In the norm, the robot reflected mass and endpoint velocity are related to the maximum estimated collision force via a simplified collision model. The reflected mass is calculated with a simplified model which differs from [8]. In order to successfully implement the safety curves provided in the ISO/TS, respectively [10], it is important to determine the robot's reflected mass sufficiently accurate, as an incorrect reflected mass can deteriorate both the human safety and performance of the system. In this paper we

- investigate the workspace effective mass distribution based on the well-established model [8] and the simplified ISO/TS model for the KUKA LWR IV+ and the Franka Emika Panda,
- conduct an experiment to derive the effective mass by observing the impulse received by an object, and
- draw implications on human safety and robot efficiency in HRI from our simulated and real-world results.

This paper is structured as follows. In Sec. II, we summarize methods to determine the reflected robot mass. For the two considered robots, we derive the workspace mass distribution in Sec. III. The experimental derivation of the reflected mass is considered in Sec. IV, implications on safe velocity control are given in Sec. IV-C. Finally, Sec. V concludes the paper.

II. EFFECTIVE MASS IN THE SAFETY CONTEXT

The robot effective mass (also referred to as the reflected mass or inertia) is the mass that an object or the human perceives during a collision. It depends on the robot's kinematic and inertial properties, the joint configuration, the joint, link, and contact elasticity as well as possibly the controller.

Consider the link side robot dynamics

$$\boldsymbol{M}(\boldsymbol{q})\ddot{\boldsymbol{q}} + \boldsymbol{C}(\boldsymbol{q},\dot{\boldsymbol{q}})\dot{\boldsymbol{q}} + \boldsymbol{g}(\boldsymbol{q}) = \boldsymbol{\tau} + \boldsymbol{\tau}_{\mathrm{ext}}\,, \tag{1}$$

where the joint and external torque are expressed as $\boldsymbol{\tau} \in \mathbb{R}^n$ and $\boldsymbol{\tau}_{\mathrm{ext}} \in \mathbb{R}^n$ and the robot's link positions and velocities are denoted $\boldsymbol{q} \in \mathbb{R}^n$ and $\dot{\boldsymbol{q}} \in \mathbb{R}^n$. The symmetric, positive

The authors are with Institute for Robotics and System Intelligence, Munich School of Robotics and Machine Intelligence, Technical University of Munich, 80797 Munich, Germany robin-jeanne.kirschner@tum.de

definite inertia matrix is $\boldsymbol{M}(\boldsymbol{q}) \in \mathbb{R}^{n \times n}$, the Coriolis matrix is $\boldsymbol{C}(\boldsymbol{q}, \dot{\boldsymbol{q}}) \in \mathbb{R}^{n \times n}$, and the gravity vector is $\boldsymbol{g}(\boldsymbol{q}) \in \mathbb{R}^{n}$. The reflected mass perceived at the point of contact in the Cartesian unit direction of impact $\boldsymbol{u} \in \mathbb{R}^3$ is given by [8]

$$m_{\mathrm{r}} = \left(\boldsymbol{u}^{\mathsf{T}} \boldsymbol{\Lambda}_{\nu}^{-1}(\boldsymbol{q}) \boldsymbol{u}\right)^{-1} , \tag{2}$$

where $\boldsymbol{\Lambda}_{\nu}^{-1}(\boldsymbol{q})$ is the upper 3×3 matrix of the robot Cartesian mass matrix inverse

$$\boldsymbol{\Lambda}(\boldsymbol{q})^{-1} = \boldsymbol{J}(\boldsymbol{q}) \boldsymbol{M}(\boldsymbol{q}) \boldsymbol{J}(\boldsymbol{q})^{\mathsf{T}} , \tag{3}$$

with $\boldsymbol{J}(\boldsymbol{q}) \in \mathbb{R}^{n \times m}$ being the Jacobian matrix at the point of contact. For rigid robots $\boldsymbol{M}(\boldsymbol{q})$, contains both the link and the motor inertia. In [15] it was shown that for the flexible joint robots like the DLR/KUKA LWR III the link inertia is decoupled from the motor inertia. In [1], the reflected robot mass was formulated as a function of the transmission stiffness

$$m_{\mathrm{r}}\left(K_J\right) = m_{\mathrm{link}} + \frac{K_J}{K_J + \gamma} m_{\mathrm{mot}} , \tag{4}$$

for the 1-DOF case[1], where m_{mot} denotes the motor inertia, m_{link} the link inertia, K_J the joint stiffness, and γ a design factor. Depending on K_J the reflected mass ranges from $m_r = m_{\mathrm{link}}$ (decoupled) to $m_r = m_{\mathrm{link}} + m_{\mathrm{mot}}$ (rigid). For planning safe motions in HRI applications the ISO/TS proposes a simplified model of the effective mass, namely

$$m_{\mathrm{r,ISO}} = M/2 + m_{\mathrm{L}} , \tag{5}$$

where M is the summed mass of all moving parts of the robot system and m_{L} is the payload [13]. Please note that (5) does not depend on the joint configuration in contrast to (2).

III. Effective mass distribution

In this section, we compare the effective masses obtained by (2) and the simplified model (5) for the reachable workspace of two exemplary robots, namely the FE Panda and the LWR IV+. No end-effector or payload is considered for both robots. We discretize the robots' reachable workspace by defining a position grid with 5 cm uniform distance, see Fig. 2 (top). We consider only one end-effector orientation, where the flange points downwards with the end-effector frame being axis-aligned with the world coordinate frame, see Fig. 2 (top left). For each position/pose in the workspace grid, we determine an associated joint configuration with the inverse kinematics algorithms [20] (LWR) and [17] (Panda). For every feasible pose/configuration we then evaluate the reflected mass in 20 uniformly distributed Cartesian directions $\boldsymbol{u}$. In Fig. 2 (top) we show the workspace grid for the LWR and Panda. The distribution of the reflected mass in the robots' workspace, i.e., the relative number of robot positions associated to a certain effective mass range is illustrated in the middle and bottom figure. Here, we also illustrate the reflected mass obtained by (5) (ISO/TS), which is simply found to be $m_{\mathrm{r,ISO}} = 5.545\,\mathrm{kg}$ for the Panda,

[1]Equation (4) may be extended to n-DOF via [16].

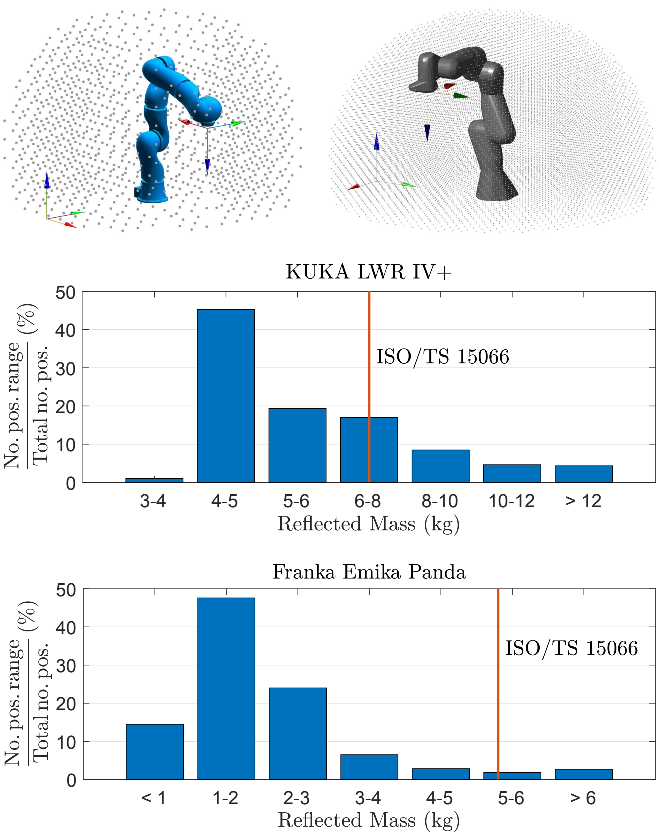

Fig. 2. Cartesian positions (top) and workspace reflected mass distribution for the KUKA LWR IV+ (middle) and Franka Emika Panda (bottom).

where we use the inertial parameters provided in [19], and $m_{\mathrm{LWR,ISO}} = 6.3\,\mathrm{kg}$ for the LWR. For the LWR it can be observed that in approx. 60 % of the reachable workspace the reflected mass is lower than the 6.3 kg obtained by ISO/TS. For the Panda, the reflected mass is lower than the simplified ISO/TS estimate in 97 % of the cases.

IV. Experimental Derivation of the Effective robot Mass

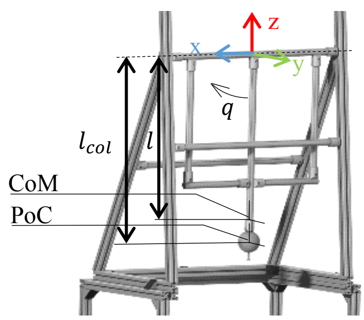

Fig. 3. Model of the pendulum's effective mass explained using it's CAD-model.

To investigate the robot effective mass experimentally, we consider the robot mass perceived during a collision with a pendulum based on the conservation of momentum

$$m_{\mathrm{p,eff}} \dot{y} = m_{\mathrm{r,exp}} v_{\mathrm{r}} , \tag{6}$$

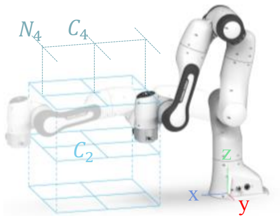

C_4	$[498, 0, 626]$ mm
N_4	$[698, 0, 626]$ mm

Fig. 4. ISO 9283 reference cube and extension for verifying the effective mass

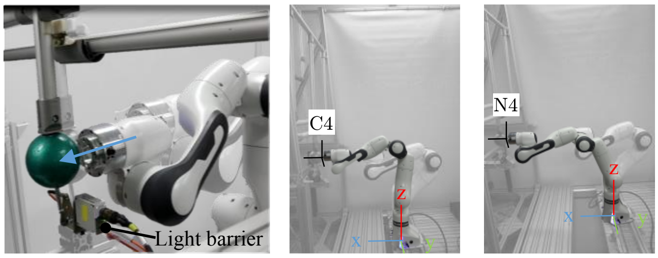

Fig. 5. Pendulum test set up to evaluate the effective mass of the robot using the depicted light barrier and a stopping mechanism at position C_4 (centre) and N_4 (right)

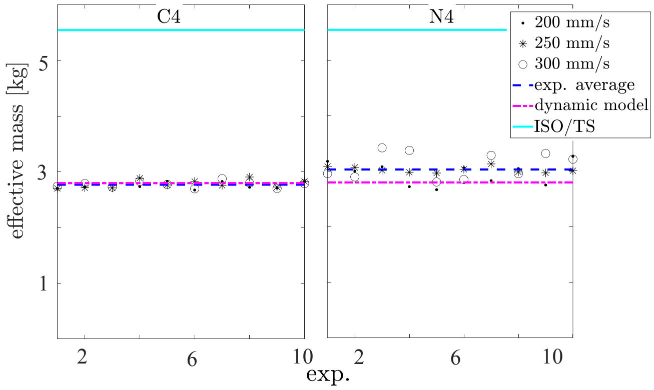

Fig. 6. Effective mass at the C_4 (left) and N_4 (right) position according to [13] (turquoise) and the experimentally derived effective mass (blue) with the corresponding values for the effective mass using [8].

where $\dot{y}$ is the pendulums instantaneous velocity after collision, $m_{\mathrm{r,exp}}$ the experimentally determined robots effective mass, v_{r} the robot velocity at the contact location.

A. Experimental setup

To obtain $m_{\mathrm{r,exp}}$ we use an experiment based on a passive physical pendulum which is shown in Fig. 3. We measure the instantaneous translational velocity $\dot{y}$ of the pendulum using a precision light barrier 203.10 and the measuring counter 373 by Hentschel. The robot velocity v_{r} at the contact location is obtained by the measured robot joint velocity, which is transformed to Cartesian space via $\boldsymbol{J}(\boldsymbol{q})$. The pendulum's effective mass at the point of contact is given by

$$m_{\mathrm{p,eff}} = \frac{J_{xx}^{(\mathrm{S})} + m_{\mathrm{p}} l^2}{l_{\mathrm{col}}^2}\,, \tag{7}$$

where $J_{\mathrm{xx}}^{(\mathrm{S})}$ is the inertia about the pendulum center of gravity, m_{p} the pendulum summed mass, $l = 636\,\mathrm{mm}$ the distance to the center of gravity, and $l_{\mathrm{col}} = 815\,\mathrm{mm}$ the distance to the point of collision. From CAD we obtain $m_{\mathrm{p,eff}} = 3.663\,\mathrm{kg}$.

We select the robot test poses based on the reference cube defined in DIN EN ISO 9283. To enable a collision with the horizontally oriented robot flange we extend the reference cube and also consider the Cartesian positions C_4 and N_4 illustrated in Fig. 4. The robot joint configurations associated to C_4 an4 N_4 are upon collision are

$\boldsymbol{q}_{C4} = [-0.9, -9.5, 0.6, -129.8, 0.8, 210.1, 51.7]^{\mathsf{T}}\ ^\circ$ and
$\boldsymbol{q}_{N4} = [-0.6, 11.9, 0.5, -92.6, 0.8, 184.8, 46.5]^{\mathsf{T}}\ ^\circ$.

We select a Cartesian robot motion along the x-axis starting close to the robot base and ending at the workspace boundary. When detecting a collision with the pendulum, the robot fully brakes triggered by the internal joint torque sensing. We use three different collision velocities: $200\,\mathrm{ms}$, $250\,\mathrm{ms}$, and $300\,\mathrm{ms}$.

In the experiment, the robot flange collides with the pendulum, we use the internal dynamics model of the Panda to calculate the effective mass according to [8] (cf. (2)) with the Cartesian direction being $\boldsymbol{u} = [1, 0, 0]^{\mathsf{T}}$.

B. Results

Our experimental results are depicted in Fig. 6. For C_4 we observe $m_{\mathrm{r,exp}} = 2.765 \pm 0.062$ kg, the difference w.r.t. (2) is $1.1\,\%$ ($m_{\mathrm{r}} = 2.797 \pm 0.003$ kg). In contrast, the error between $m_{\mathrm{r,exp}}$ and the ISO/TS effective mass $m_{\mathrm{r,ISO}} = 5.22\,\mathrm{kg}$ is $88.8\,\%$. We obtain similar results for the N_4 position, i.e. $m_{\mathrm{r,exp}} = 3.018 \pm 0.184$ kg in the experiment, $m_{\mathrm{r}} = 2.800 \pm 0.005$ kg via (2), and $m_{\mathrm{r,ISO}} = 5.222$ kg (ISO/TS) where the error between experiment and (2) is $7.8\,\%$ and $73.0\,\%$ between experiment and ISO/TS.

The error between experiment and (2) in our N_4 experiments is higher than in the C_4 experiment. This is presumably due to the preliminary experimental set up, which requires further calibration. Please also note that the Panda internal robot model is closed, i.e., not available to the authors, and may differ from the model used in Sec. III.

C. Usage of incorrect mass for safe velocity control: Implications on safety and performance

Inspired by [10], the ISO/TS provides safety curves which relate the instantaneous robot reflected mass to a maximum biomechanically safe velocity (pain threshold). Consider the following two undesired scenarios:

a) The actual robot mass is lower than the mass calculated according to ISO/TS. The commanded velocity is regarded as safe, but a higher safe velocity would be possible based on the actual robot reflected mass. In this case, productivity is deteriorated in terms of cycle time.
b) The robot reflected mass is larger than the one obtained by ISO/TS, the robot travels with a speed that is higher than the safety curve would allow based on the actual

mass. The safety thresholds may be violated, which potentially makes the application unsafe.

According to our results in Sec. III, case a) holds for 97 % of the workspace area of the FE Panda and for more than 60 % of the workspace of the KUKA LWR IV+. For these robots, the application of the ISO/TS reflected mass usually results in decreased productivity. However, also case b) is likely, meaning the safety thresholds can be exceeded. The authors therefore recommend to replace the effective mass model (5) in ISO/TS by the well-established formulation (2) [8] (as our experimental results agree well with the theory for the considered robots) or a data-driven relation between the robot configuration and the measured reflected mass.

V. Conclusion

The effective mass of a robot is known to have an important impact on the operator safety in case of a collision. In our experimental investigations we observed a significant difference between the simplified ISO model and the state of the art dynamic model that is well established in the robotics community since decades. The simplified model proves to be not only overly conservative in most cases, thereby limiting the robot's efficiency and economic use, but it may also lead to an underestimation of hazard, which can jeopardize human safety in HRI applications. Therefore, we suggest for every collaborative robot to provide and use an accurate dynamics model for appropriate real-time safety control and reliable safety assessment.

ACKNOWLEDGMENT

The authors would like to thank Johanna Wolff for her preparatory work. This work was supported by the European Union's Horizon 2020 research and innovation programme as part of the project ILIAD under grant no. 732737 and partially supported by the Research Project I.AM. through the European Union H2020 program under GA 871899. We gratefully acknowledge the funding of the Lighthouse Initiative Geriatronics by StMWi Bayern (Project X, grant no. 5140951) and LongLeif GaPa gGmbH (Project Y, grant no. 5140953). Please note that S. Haddadin has a potential conflict of interest as shareholder of Franka Emika GmbH.

References

[1] A. Bicchi and G. Tonietti, "Fast and "soft-arm" tactics," in IEEE Robotics & Automation Magazine, vol. 11, no. 2, pp. 22-33, June 2004.

[2] R. Behrens and N. Elkmann, "Study on meaningful and verified Thresholds for minimizing the consequences of human-robot collisions," 2014 IEEE International Conference on Robotics and Automation (ICRA), Hong Kong, 2014, pp. 3378-3383.

[3] S. Haddadin, A. Albu-Schffer, O. Eiberger and G. Hirzinger, "New insights concerning intrinsic joint elasticity for safety," 2010 IEEE/RSJ International Conference on Intelligent Robots and Systems, Taipei, 2010, pp. 2181-2187.

[4] K. Suita, Y. Yamada, N. Tsuchida, K. Imai, H. Ikeda and N. Sugimoto, "A failure-to-safety "Kyozon" system with simple contact detection and stop capabilities for safe human-autonomous robot coexistence," Proceedings of 1995 IEEE International Conference on Robotics and Automation, Nagoya, Japan, 1995, pp. 3089-3096 vol.3.

[5] S. Haddadin, A. Albu-Schäffer, G. Hirzinger, "Safety Evaluation of Physical Human-Robot Interaction via Crash-Testing." Robotics: Science and systems, vol. 3, 2007.

[6] K. Ikuta, H. Ishii, M. Nokata, Safety Evaluation Method of Design and Control for Human-Care Robots. The International Journal of Robotics Research. 2003;22(5):281-297.

[7] O. Khatib, "A unified approach for motion and force control of robot manipulators: The operational space formulation," in *IEEE Journal on Robotics and Automation*, vol. 3, no. 1, pp. 43-53, February 1987.

[8] O. Khatib, "Inertial Properties in Robotic Manipulation: An Object-Level Framework." *The International Journal of Robotics Research*. 1995;14(1):19-36.

[9] D. Walker, "The use of kinematic redundancy in reducing impact and contact effects in manipulation", Robotics and Automation 1990. Proceedings. 1990 IEEE International Conference on, pp. 434-439, 1990.

[10] S. Haddadin, S. Haddadin, A. Khoury, T. Rokahr, S. Parusel, R. Burgkart, A. Albu-Schäffer, "On making robots understand safety: Embedding injury knowledge into control", *The International Journal of Robotics Research*, vol. 31, 13th ed, 2012, pp. 1578-1602.

[11] D. Kulić, E. Croft, "Pre-collision safety strategies for human-robot interaction." Auton Robot, vol. 22, 2007, pp. 149164.

[12] N. Mansfeld, B. Djellab, J. R. Veuthey, F. Beck, C. Ott and S. Haddadin, "Improving the performance of biomechanically safe velocity control for redundant robots through reflected mass minimization," 2017 IEEE/RSJ International Conference on Intelligent Robots and Systems (IROS), Vancouver, BC, 2017, pp. 5390-5397.

[13] ISO/TS 15066:2017, *Robots and robotic devices - Collaborative robots*, Beuth-Verlag, Berlin.

[14] T. Lens and O. von Stryk, "Investigation of safety in human-robot-interaction for a series elastic, tendon-driven robot arm," 2012 IEEE/RSJ International Conference on Intelligent Robots and Systems, Vilamoura, 2012, pp. 4309-4314.

[15] S. Haddadin, et al. Requirements for Safe Robots: Measurements, Analysis and New Insights. The International Journal of Robotics Research, vol. 28, no. 1112, Nov. 2009, pp. 15071527.

[16] A. Albu-Schaffer, M. Fischer, G. Schreiber, F. Schoeppe and G. Hirzinger, "Soft robotics: what Cartesian stiffness can obtain with passively compliant, uncoupled joints?," 2004 IEEE/RSJ International Conference on Intelligent Robots and Systems (IROS) (IEEE Cat. No.04CH37566), Sendai, 2004, pp. 3295-3301, vol.4.

[17] P. Corke, Robotics, vision and control: fundamental algorithms in MATLAB second, completely revised. Vol. 118. Springer, 2017.

[18] W. J. Stronge, "Impact mechanics." Cambridge university press, 2018.

[19] C. Gaz, M. Cognetti, A. Oliva, P. Robuffo Giordano and A. De Luca, "Dynamic Identification of the Franka Emika Panda Robot With Retrieval of Feasible Parameters Using Penalty-Based Optimization," in IEEE Robotics and Automation Letters, vol. 4, no. 4, pp. 4147-4154, Oct. 2019.

[20] R. Konietschke, Planning of Workplaces with Multiple Kinematically Redundant Robots, Technical University of Munich, 2008.